International Journal of Biological Macromolecules 151 (2020) 566–575

Contents lists available at ScienceDirect

International Journal of Biological Macromolecules

journal homepage: http://www.elsevier.com/locate/ijbiomac

A highly sensitive label-free amperometric biosensor for norfloxacin detection based on chitosan-yttria nanocomposite

Amit K. Yadav [a], Tarun K. Dhiman [a], G.B.V.S. Lakshmi [a], Anna N. Berlina [b], Pratima R. Solanki [a,*]

[a] Special Centre for Nanoscience, Jawaharlal Nehru University, New Delhi 110067, India
[b] Immunobiochemistry laboratory, A.N. Bach Institute of Biochemistry, Research Center of Biotechnology of the Russian Academy of Sciences, Moscow 119071, Russia

ARTICLE INFO

Article history:
Received 27 December 2019
Received in revised form 31 January 2020
Accepted 10 February 2020
Available online 11 February 2020

Keywords:
Antibiotic resistance
Anti-fluoroquinolones
Chitosan
Immunosensor
Norfloxacin
Yttrium oxide

ABSTRACT

Here, non-invasive and label-free detection of trace-level of norfloxacin (NF) in human urine samples has been reported using the electrochemical technique. Nanostructured yttrium oxide (nY_2O_3) was synthesized at low-temperature using a one-step hydrothermal process. These nY_2O_3 were characterized by various methods including XRD, FT-IR, Raman spectroscopy, and TEM. A biosensing platform based on nY_2O_3 modified with chitosan (CH) was fabricated for the detection of NF. The nanocomposite film (CH-Y_2O_3/ITO) was characterized by FE-SEM, contact angle measurements, and electrochemical techniques. Further, fluoroquinolones antibodies (anti-FQ) were used to modify the CH-Y_2O_3/ITO electrode *via* covalent interaction. Non-specific sites were blocked by bovine serum albumin (BSA), those present on the anti-FQ/CH-Y_2O_3/ITO electrode surface. The response study of BSA/anti-FQ/CH-Y_2O_3/ITO bioelectrode towards NF detection revealed a wide range (1 pM-10 μM) with a lower detection limit of 3.87 pM using differential pulse voltammetry (DPV). The sensitivity obtained is as high as 10.14 μA μM^{-1} cm^2 with a fast response time of ~10 min. Moreover, the diagnostic performance of the fabricated sensor was evaluated to detect NF in urine spiked sample. The recovery of NF from the spiked sample was observed from 90.5 to 101.1%, with a maximum relative standard deviation of 7.04. The obtained results of the fabricated bioelectrode (BSA/anti-FQ/CH-Y_2O_3/ITO) was validated with ELISA. The results were found better when compared with earlier described biosensors and commercially existing ELISA in terms of sensitivity and lower detection limit.

1. Introduction

The advent of β-lactam antibiotics for the treatment of numerous communicable diseases in humans as well as in animals marked the beginning of the era of antimicrobial therapy in 1940s. Antibiotics are mainly used because of their specific activity to counter gram-positive and gram-negative bacteria. Globally, India ranks first, followed by China and the USA, in consuming antibiotics [1]. This overuse of drugs leads to antibiotic resistance in bacteria, which became a challenging problem in many areas like health centers, hospitals, and in societies because of an overall increase in the number of patients and the associated cost of treatment [2,3]. In future, the phenomena of antibiotic resistance will be more challenging. The inability to diagnose bacterial infections is the prime restraining factor, which leads to inappropriate use of antibiotics and a decrease in the survival rate during septic conditions. Therefore, there is a need to monitor the usage and release of these drugs into the environment through the human body.

Norfloxacin (NF) is a member of fluoroquinolone (FQ) antibiotics of the third generation and with chemical name 1-ethyl-6-fluoro-1,4-dihydro-4-oxo-7-(piperazine-1-yl) quinolone-3-carboxylic acid. It is the first choice to treat various infectious illnesses caused by *E. coli*, *Campylobacter*, *Salmonella shigella*, and *V. colera* [4,5]. The properties like the 6^{th} positioned fluorine atom in NF offers amplified potency to counter gram-negative bacteria, and the position of piperazine moiety at 7^{th} place are the reasons for the anti-pseudomonal action of NF [6]. It's well known that extensive use of antibiotics will eventually lead to more and more organisms becoming resistant [7]. The various non-target toxic effects of NF have also been reported in the earlier works published [8]. As far as human health is concerned, the detection of NF in clinical and biological samples is of utmost importance because of its potentially toxic effects. NF has been detected by sequential analytical methods like fluorometry [9], spectrophotometry [10], and high-performance liquid chromatography (HPLC) [11–17]. Though HPLC has been extensively used owing to its selectivity, susceptibility, and capability to diminish interferences, but it is time-taking, requires wide solvent-usage and high-class devices, with a high maintenance cost which limits its usage. Electrochemical detection of an analyte based on nanomaterial modified electrodes is a precise method in analytical chemistry for the determination of biomolecules and drugs [18,19]. In the previously reported literature, very few studies have involved the electrochemical method for the determination of NF [20,21]. New

* Corresponding author.
E-mail addresses: partima@mail.jnu.ac.in, pratimarsolanki@gmail.com (P.R. Solanki).

https://doi.org/10.1016/j.ijbiomac.2020.02.089
0141-8130/

methods for the detection of NF are therefore needed to develop, with having high speed, specificity, robustness, low-cost, and easy to handle instrumentation.

Biosensors have an outstanding performance capability such as high accuracy and precision, low cost, quick response, user-friendly operation, reliability, relatively compact size, and continuous real-time assessment [22]. Nanoparticles (NPs) are currently used to enhance the overall quantitative performance of electrochemical biosensors for biological and chemical detection [23]. Due to the exciting nanoscale morphology, non-toxicity, and catalytic properties, nanosized metal oxides (NMOs) have attracted significant interest among the various types of nanomaterials developed as immobilizing matrices for the development of biosensors. Optimized rare earth metal oxide NPs could be useful for nanobiosensors/sensors, bioprobes, drug discovery, genetic analysis, medical diagnostics, flow cytometry, and high-throughput screening [24]. They can easily be used for non-invasive, nondestructive, and real-time in vivo diagnosis of numerous ailments. Among them, the nanostructured yttrium oxide (nY_2O_3) has recently awakened much interest as biological immobilization matrix due to its excellent properties such as its high dielectric constant, chemical inertness, thermal stability, high surface-to-volume ratio, extremely rapid mobility of ions, charge transfer capability, biocompatibility, wide bandgap and interesting electrochemical properties making it a suitable biosensing material [25,26]. The thin film of yttrium oxide become strongly conductive due to the low dielectric constant (13) value, which make it a probable aspirant for application towards the biosensors development [27]. Besides this, the nY_2O_3 is a desirable inorganic metal oxide consisting of yttrium and oxygen elements. The oxygen moieties in nY_2O_3 help in the functionalization and covalent immobilization of antibodies. However, the major problem of the agglomeration of nY_2O_3 onto a specific matrix containing biological molecules has led to limited biosensing applications. This issue can be overcome by modifying nY_2O_3 with chitosan (CH), biopolymer matrix to develop a nanocomposite film so that they are adequate for biosensor application [28–31]. CH has an excellent ability to form films, biocompatible and biodegradable polymer, and is widely adopted in the nanocomposite fabrication for immobilization of biomolecules by affixing covalently to their amino/hydroxyl groups [32–35].

In this article, a rare earth metal oxide, nY_2O_3 has been synthesized using a one-step hydrothermal synthesis method to develop a susceptible and highly sensitive biosensing platform for the detection of NF. It is found that the CH-Y_2O_3 composite is not yet reported in the literature for electrochemical devices. This fabricated BSA/anti-FQ/CH-Y_2O_3/ITO bioelectrode exhibited higher sensitivity and low detection limit (3.87 pM), when compared with previously described immunosensors and also commercially available enzyme-linked immunosorbent assay (ELISA) towards the detection of the NF.

2. Experimental

2.1. Reagents and materials

High purity yttrium nitrate [$Y(NO_3)_3.6H_2O$], 1-(3-(dimethylamino)-propyl)-3-ethylcarbodiimide hydrochloride (EDC), acetonitrile, bovine serum albumin (BSA) were procured from Sigma Aldrich. Potassium hydroxide, acetone, hydrogen peroxide (H_2O_2), and ethanol obtained from Fisher Scientific. Chitosan (medium molecular weight: 190–310 kDa, viscosity: 298 mPa s, deacetylation degree: 90.12%, structural composition: $(C_6H_{11}NO_4)_n$, Sodium hydroxide pellets (NaOH), norfloxacin antigen (NF), sodium monophosphate anhydrous [NaH_2PO_4], sodium diphosphatedihydrate [$Na_2HPO_4.2H_2O$], potassium ferricyanide ($K_3[Fe(CN)_6]$), potassium ferrocyanide ($K_4[Fe(CN)_6]3H_2O$), uric acid, and urea were purchased from SRL Limited. Cetyltrimethylammonium bromide (CTAB) and N-hydroxysulfosuccinimide (NHS) [$C_4 H_5 NO_3$] were procured from HiMedia and SpectroChem, respectively. The glass substrate fully covered with Indium Tin Oxide (ITO) (Baltracom 247 ITO, transmittance 90%, with sheet resistance 25 Ω sq.$^{-1}$) purchased from Balzers, UK. All of other chemicals were of analytical-grade, which were used without further purification. The fresh phosphate buffer solution (PBS; 50 mM) with pH 7.0 was formed with [NaH_2PO_4] (0.05 mol L^{-1}) and [$Na_2HPO_4.2H_2O$] (0.05 mol L^{-1}) in deionized water (DI) and kept at 4 °C. The anti-fluoroquinolones (anti-FQ) antibodies (host sheep) were taken from MyBiosource, USA, and have further diluted in PBS, having pH 7.0. ELISA Kit was purchased from Elabscience (Cat. No. E-FS-E074) Indian distributer.

2.2. Synthesis of nanostructured Yttria (nY_2O_3) and its modification with chitosan

The hydrothermal method was used for the synthesis of nY_2O_3. Briefly, 30 mM $Y(NO_3)_3.6H_2O$, 90 mM of NaOH, and 15 mM CTAB solutions were prepared in DI separately through constant stirring. NaOH solution was dropped slowly into the solution of $Y(NO_3)_3.6H_2O$ under continuous stirring (300 rpm) at room temperature (RT, 25 °C) until the pH became 10. After that CTAB solution was added dropwise to the above mixture under stirring (300 rpm) for 2 h. The final prepared solution was transferred into a Teflon vessel and placed in hydrothermal pressure assembly. Further, this set-up was kept at 170 °C for 20 h in a muffle furnace to carry out the hydrothermal process, and the obtained precipitate was allowed to cool [Scheme 1(a)]. The obtained precipitate was washed until the pH reached to neutral using DI water and centrifugation process (4500 rpm at an interval of 15 min). Afterward, the attained solid was dried at 60 °C overnight and further annealed at 600 °C for 4 h. Finally, the acquired product was ground to a fine powder in mortar-pestle and used for study. The nY_2O_3 (1 mg mL^{-1}) was dispersed in a solution of 1% CH [prepared using acetic acid (1%)] under vigorous stirring at room temperature to prepare the CH-Y_2O_3 nanocomposite.

2.3. Fabrication of biosensing platform

All ITO coated glass substrates of the similar size (0.5 × 1.5 cm) were selected and hydrolyzed by keeping them in the solution mixture of H_2O: NH_4OH: H_2O_2 in the ratio of 5:1:1 for 1 h at 80 °C and washed with DI water & ethanol and dried at 60 °C. Freshly prepared CH-Y_2O_3 solution (30 μL) was drop-casted in an area of 0.25 cm^2 onto the hydrolyzed ITO substrate and dried at 60 °C, represented as CH-Y_2O_3/ITO electrode. Likewise, the CH solution was also drop casted on the surface of the ITO (CH/ITO electrode) for comparative analysis. A solution of anti-FQ (50 μM) was prepared in PBS (pH 7.0). Also, a solution containing EDC (0.4 M) and NHS (0.1 M) was prepared in PBS (pH 7.0). Next, a final solution was prepared with anti-FQ (50 μg mL^{-1}): EDC: NHS in 2:1:1 ratio, and incubated for 45 min prior use. The 30 μL of the above solution was spread uniformly onto CH-Y_2O_3/ITO electrode using the drop-casting method and maintained for almost 6 h in a humid chamber at RT. The anti-FQ was covalently bound on CH-Y_2O_3/ITO by forming bond between -NH_2 group of CH molecules and carboxyl group (–COOH) on Fc portion of anti-FQ. EDC activated the –COOH of anti-FQ during the reaction and made an unstable O-acylisourea ester, and this ester reacted to NHS, produced an amine-reactive NHS ester, which is a stable intermediate product. These NHS activated anti-FQ support to connect with –NH_2 groups present on CH molecules to form an amide bond. The unbound antibodies removed from the anti-FQ/CH-Y_2O_3/ITO bioelectrode by washing with PBS (200 μL) of pH 7.0. Lastly, the non-specific sites present on the bioelectrode were blocked by dropping 10 μL BSA (1 mg mL^{-1}) and kept again in the humid chamber for 2 h. The engineered BSA/anti-FQ/CH-Y_2O_3/ITO bioelectrode was washed with PBS and kept at 4 °C for later use. NF solutions were prepared using PBS (pH 7) using a serial dilution method in the range from 1 pM to 10 μM. Schematic of the fabrication of nanocomposite and bioelectrode based on CH-Y_2O_3 was shown in Scheme 1(b).

(a)

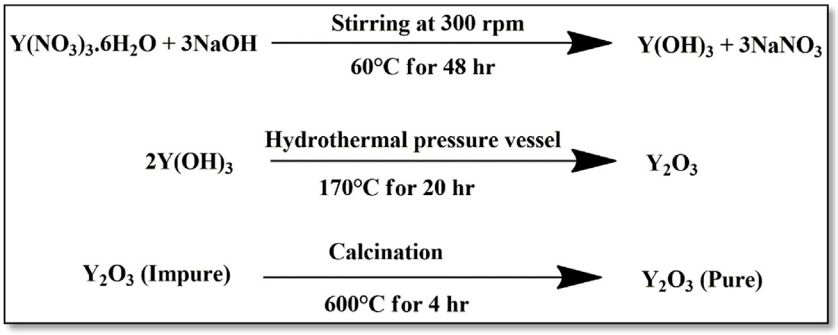

(b)

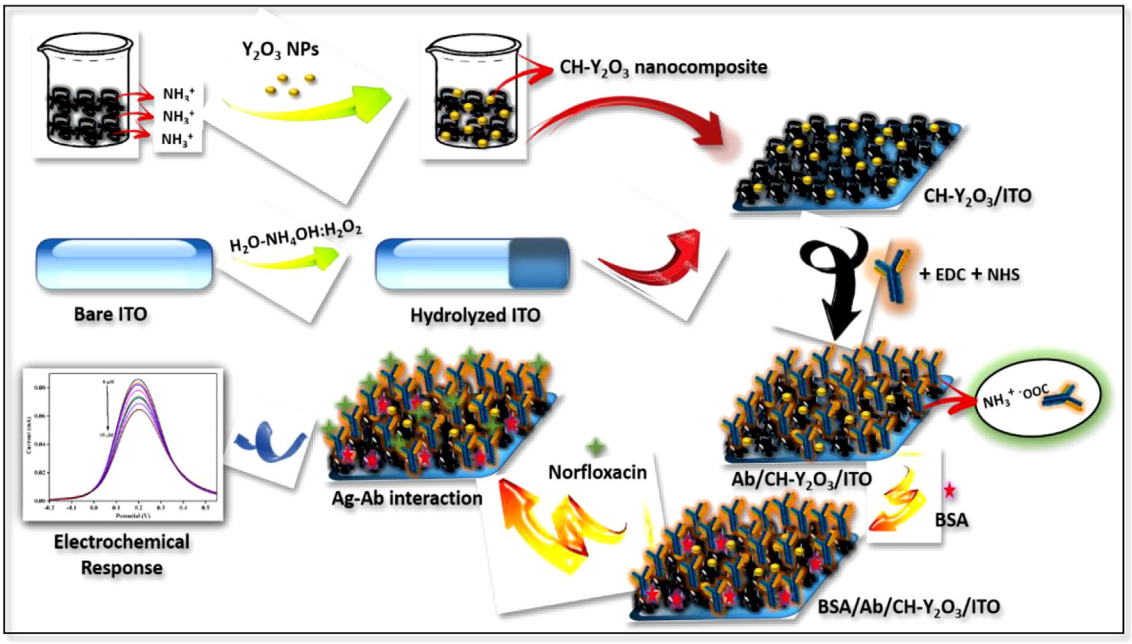

Scheme 1. a) Chemical synthesis of nY_2O_3; b) Fabrication process of BSA/anti-FQ/CH-Y_2O_3/ITO bioelectrode for detection of NF.

2.4. Preparation of urine spiked sample

The spiked samples of human urine were prepared by mixing 20 μL of human urine in 3 mL of PBS (pH 7.0) comprising 5 mM $[Fe(CN)_6]^{3-/4-}$ with different concentrations of NF (1, 10, 100 pM; 1, 10, 100 nM; and 1 and 10 μM). These spiked samples were used for sensing measurements through BSA/anti-FQ/CH-Y_2O_3/ITO bioelectrode.

2.5. Instrumentation

The phase structure and crystalline nature of nY_2O_3 were investigated by X-ray diffractometer (XRD) [Rigaku Miniflex 600 (Japan) diffractometer having Cu-Kα radiation with a monochromatic X-ray beam at $\lambda = 1.5406$ Å]. The data has been gathered in an angular range of 10–80° (2θ), having a step size of 5° (2θ) at RT, and the obtained results were evaluated by using EVA software. The modification of nY_2O_3 with CH and immobilization of anti-FQ on the CH-Y_2O_3/ITO electrode was confirmed by using Fourier transform infrared spectroscopy (FT-IR, Perkin Elmer, US). Morphology and structural studies were performed by using high-resolution transmission electron microscopy (HR-TEM, JEM-2200 FS, Jeol, Japan). For this, the sample was prepared by ultrasonic dispersion of nY_2O_3 in ethanol. The dispersion was drop-casted on carbon-coated copper grid and then dried at RT for overnight. To investigate the topographical and elementary information of electrodes of CH/ITO electrode, Y_2O_3/ITO electrode, CH-Y_2O_3/ITO electrode, and anti-FQ/CH-Y_2O_3/ITO bioelectrode, the study of field emission-scanning electron microscopy (FE-SEM) was carried out. Raman frequency for nY_2O_3 was confirmed on EnSpectr R532 (US). The absorbance of nY_2O_3 was measured by using T90+ UV/VIS spectroscopy. The change in hydrophilic/ hydrophobic behavior of ITO, CH/ITO, CH-Y_2O_3/ITO, and anti-FQ/CH-Y_2O_3/ITO electrodes were investigated by contact angle (CA) study, carried out on SURFTENS universal instrument (OEG GmbH Germany). All electrochemistry measurements [cyclic voltammetry (CV), frequency response analysis (FRA) and differential pulse voltammetry (DPV)] was done using an Autolab Galvanostat/Potentiostat electrochemical analyzer (EcoChemie, The Netherlands) attached to a separate computer and managed by the NOVA (version 1.10) software. All the measurements were carried out in PBS (0.1 M, pH 7.0), comprising 5 mM $[Fe(CN)_6]^{3-/4-}$ as the electrolyte utilizing the three-electrode system with Ag/AgCl as a reference electrode.

3. Results and discussion

3.1. Structural characterizations

XRD was performed to study the phase, crystallinity, and structure of the nY_2O_3. Fig. 1(a) shows the obtained XRD plot for a 2θ angle ranging from 10 to 80°. The characteristic peaks were obtained at 29.2°, 48.5°, and 57.6° marked corresponding to (222), (440) and (622) planes. Few minor peaks were also found at 20.5° (211), 33.8° (400), 35.9° (411), 39.8° (332), 43.5° (431), 53.2° (611), and 59.0° (631). It was observed that these peaks of diffraction precisely matched with the JCPDS No. 41–1105, indicating the presence of the cubic phase of nY_2O_3 [36,37]. The average crystallite size of nY_2O_3 was obtained to be ~ 11 nm calculated using the Debye-Scherrer equation corresponding to the highest intensity peak (222).

$$D = \frac{0.9\lambda}{\beta\cos\theta} \quad (1)$$

where $\lambda = 1.540$ Å ($Cu\text{-}K_\alpha$ wavelength), β - full width at half maximum (FWHM), and θ - diffraction angle of the diffraction peak.

Raman spectroscopy was used to study the phase and surface defects of nY_2O_3. Fig. 1(b) shows the Raman spectrum of nY_2O_3. The sharp peak at 375 cm^{-1} corresponds to the cubic structure of nY_2O_3. Weak peaks were also obtained at 327 cm^{-1}, 417 cm^{-1}, 467 cm^{-1}, and 592 cm^{-1} correspondings to cubic nY_2O_3. These results are in agreement with the results obtained through XRD and similar results reported on the nY_2O_3 Raman spectrum [38–40].

The size and morphology of synthesized nY_2O_3 were examined using transmission electron microscopy (TEM) [Fig. 2 (a-d)]. The TEM image at lower magnification showed that the synthesized nanoparticles were agglomerated, and no defined shape was observed, as shown in Fig. 2 (a,b). Nanoparticles generally tend to clump together because of their smaller sizes and high surface energy [41]. Fig. 2 (c, d) was typical high-resolution TEM image (HR-TEM) and selected area

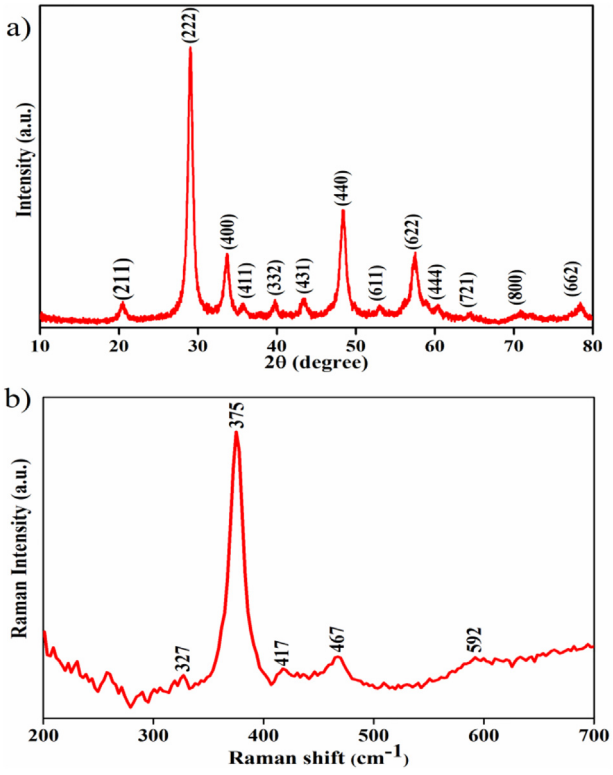

Fig. 1. (a) X-ray diffraction pattern of nY_2O_3 and (b) Raman scattering spectrum of the nY_2O_3.

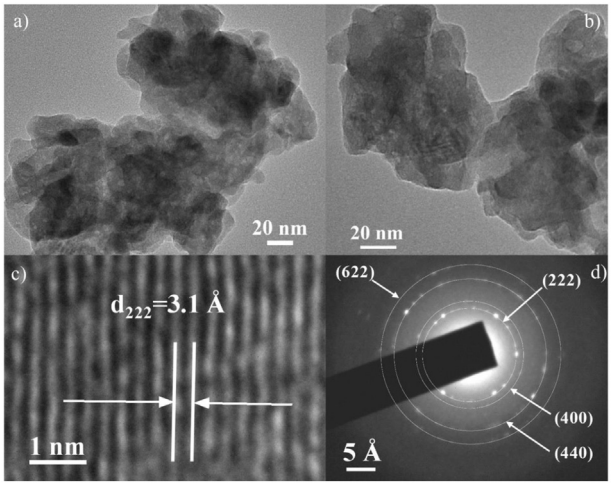

Fig. 2. (a) and (b) TEM images; c) SAED pattern, and d) HR-TEM image of nY_2O_3.

electron diffraction (SAED) patterns of nY_2O_3. The SAED pattern of the nY_2O_3 indicated that they are polycrystalline. The lattice fringes were well defined and had a d-spacing of 0.32 nm, representing the plane (222) of the cubic nY_2O_3. These observations correspond to the d-values, calculated from the XRD studies for the respective planes. Also, the SAED pattern showed the highly crystalline nature of nY_2O_3, and the spots obtained were well indexed to (211), (222), (431), and (440) planes of cubic nY_2O_3 (JCPDS card 41-1105). In HR-TEM also the nanocrystalline nature of nY_2O_3 was observed. The d spacing was found to be 3.2 Å that corresponds to (222) plane.

3.2. FT-IR, Contact angle and FE-SEM studies

Fig. 3 represents the FT-IR spectra of (a) CH/ITO electrode, (b) nY_2O_3/ITO electrode (c) CH-Y_2O_3/ITO electrode, and (d) anti-FQ/CH-Y_2O_3/ITO bioelectrode. In the spectrum (a) the peak at 1545 cm^{-1} was assigned to -NH_2 group, and 1149 cm^{-1} was of β (1–4) glycosidic group in polysaccharide units, which are present in CH. The peak at 1016 cm^{-1} represents C—O stretch; 1070 and 1404 cm^{-1} arose because of C—N stretch of C-NH_2 in CH [42,43]. In spectra (b and d), O—H stretching appears at 3000 cm^{-1} (broadband), and few peaks of -NH_2 group also were present. In spectrum (b), the peak corresponds to Y—O bond appeared at 555 cm^{-1} [44,45], and the peaks seemed at 1510, and 1070 cm^{-1} represent the –COOH groups, which may be due to CO_2 absorption in air when exposed [46–48]. In spectrum (c), the bands corresponding to CH exist along with a weak peak at 555 cm^{-1}

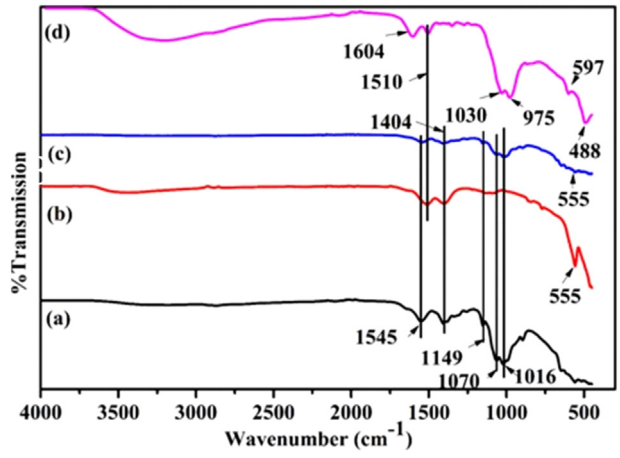

Fig. 3. FTIR spectra of (a) CH/ITO; (b) nY_2O_3/ITO; (c) CH-Y_2O_3/ITO; and (d) anti-FQ/CH-Y_2O_3/ITO bioelectrode.

co-exist, confirming the formation of CH-Y_2O_3 composite formation. In spectrum (d), after the immobilization of the anti-FQ, the peak corresponding to Y—O band appeared at 555 cm^{-1} shifted, and another peak of Y—O at 464 cm^{-1} also shifted to higher wavenumber side. Even the peaks corresponding to –COOH were also found to be shifted. These results established the anti-FQ immobilization on CH-Y_2O_3 surface. A peak near 1600 cm^{-1} corresponding to -NH_2 in amino acid appeared showing the presence of anti-FQ.

The wettability of the electrode's surface and hydrophilicity depend heavily on the chemistry of that surface. Since the operative charges persist on the electrode surface, the wettability measurement is essential. For this, water contact angle (CA) was measured in a static state for nY_2O_3/ITO electrode, CH/ITO electrode, CH-Y_2O_3/ITO electrode, and anti-FQ/CH-Y_2O_3/ITO bioelectrode [Fig. 4]. A water drop was placed on each electrode surface using a syringe, and the contact angle was quantified at the interface of the electrode surface. The measured value of the nY_2O_3/ITO contact angle was 109°, indicating the hydrophobic nature [Fig. 4 (a)]. The CA of CH/ITO electrode was measured as 72° [Fig. 4 (b)], showing slightly hydrophilic nature as compared to nY_2O_3/ITO. The CA of CH modified nY_2O_3 (CH-Y_2O_3/ITO) electrode was obtained to be 70° showing hydrophilic behavior with drastic change [Fig. 4 (c)] as compared to nY_2O_3/ITO electrode. This improved hydrophilic behavior of the CH-Y_2O_3/ITO electrode provides an extremely favorable condition for immobilization of anti-FQ. Following the immobilization of anti-FQ on CH-Y_2O_3/ITO electrode [Fig. 4 (d)], the contact angle value was decreased to 33°, showing the increase in the hydrophilic nature of anti-FQ/CH-Y_2O_3/ITO bioelectrode due to the covalent interaction between the anti-FQ and CH-Y_2O_3/ITO electrode.

FE-SEM images are shown in Fig. 5. The porous surface of CH defined its polymeric nature [Fig. 5 (a)]. Fig. 5 (b) displays the uniformly dispersed grains of nY_2O_3 with a high degree of agglomeration. Fig. 5 (c) shows the porous globular microstructure after the integration of nY_2O_3 with CH molecules, which confirms the formation of CH-Y_2O_3 nanocomposite. This may demonstrate that the surface charge of nY_2O_3 is evenly self-assembled via intermolecular interactions and hydrogen bonds on the cationic network of CH and harsh porous morphology, which appear to provide a friendly environment for antibodies immobilization. The further increase in grain boundaries of the electrode anti-FQ/CH-Y_2O_3/ITO and the structure of antibodies like globules [Fig. 5 (d)] reveals the uniform biomolecule's immobilization on the surface of the electrode CH-Y_2O_3/ITO.

3.3. Electrochemical studies

Confirmational alterations in the structure of biomolecules are known to occur due to extreme pH which hindered the interaction between antibody and antigen. Thus, the influence of pH was defined before the electrochemical experiments to analyze the electrochemical

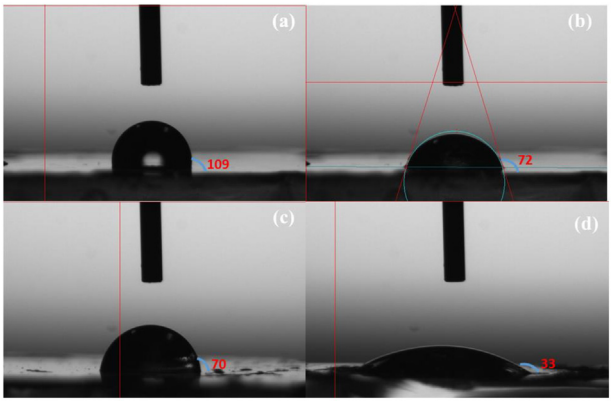

Fig. 4. Contact angle measurements of (a) nY_2O_3/ITO; (b) CH/ITO; (c) CH-Y_2O_3/ITO; and (d) anti-FQ/CH-Y_2O_3/ITO bioelectrode.

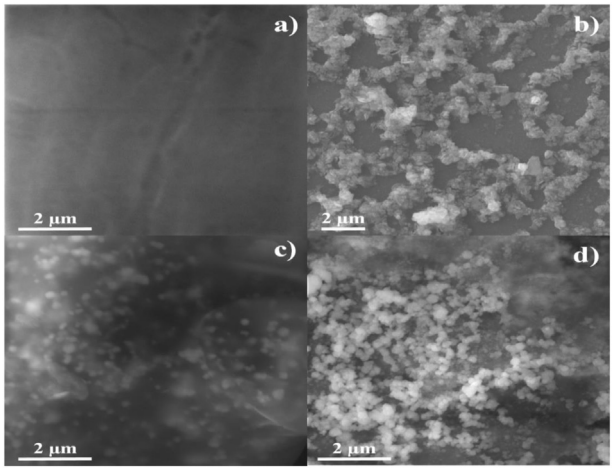

Fig. 5. FE-SEM images of (a) CH/ITO; (b) nY_2O_3/ITO; (c) CH-Y_2O_3/ITO; and (d) anti-FQ/CH-Y_2O_3/ITO bioelectrode.

behavior of antibodies present on the surface of fabricated immunoelectrode through DPV using PBS of various pH (6.0–8.0) containing 5 mM of $[Fe(CN)_6]^{3-/4-}$ ions. The highest peak of current was observed at pH 7.0 [Fig. 6A]. This might be because of biological entities such as enzyme, antibody, antigen, amino acid, etc. show intense activity at relatively neutral pH in their pure form. In case of acidic or basic pH, the amino acid sequence of antibodies, interacting with H^+ or OH^- ions may have been denatured their structure [49,50]. Thus, all the electrochemical experiments were done at pH 7.0.

Fig. 6B shows the DPV curves of the CH/ITO electrode (curve i), CH-Y_2O_3/ITO electrode (curve ii), anti-FQ/CH-Y_2O_3/ITO bioelectrode (curve iii) and BSA/anti-FQ/CH-Y_2O_3/ITO (curve iv) bioelectrode to confirm the stepwise immobilization of biomolecule on the electrode surface. CH/ITO electrode produced the lowest peak current (curve i; 0.0293 mA). The deposition of CH-Y_2O_3 on ITO electrode increased this current to 0.032 mA because of the increased electron transfer between medium and CH-Y_2O_3/ITO electrode (curve ii). The current increase was further observed after the immobilization of anti-FQ on CH-Y_2O_3/ITO surface (curve iii; 0.0533 mA). This demonstrated that FQ antibodies shows mediator like activity between the electrode and the electrolyte due to the significant shortening of electron tunneling distance between antibodies. Along with this, the fast electron diffusion towards the bioelectrode takes place because of the electronic interaction between the free sites on the antibodies (-NH_2 terminal) and the redox species $[Fe(CN)_6^{3-/4-}]$ [51,52]. The peak current further increased to 0.0850 mA (curve iv) after the anti-FQ/CH-Y_2O_3/ITO bioelectrode was blocked with BSA [53,54]. The zwitterionic natured of BSA is interacting with the metal oxide and thereby changing the isoelectric point at the electrode-electrolyte interface, which may cause current increase [55,56]. Also, the interaction between BSA with metal ions may help in the creation of electron transfer path between the electron-rich electrolyte and the bioelectrode leading to an increase in the current. The CV studies provide the same conclusion as described in supplementary information.

The electro-kinetics of CH-Y_2O_3/ITO electrode and BSA/anti-FQ/CH-Y_2O_3/ITO bioelectrode at the interface of the electrode surface and electrolyte were examined by *CV* using a scan rate of 10 to 100 mV/s (Fig. 6 C & D). For both electrodes, the anodic peak current to the cathodic peak current (Ipa/Ipc) ratio projected at 50 mV/s was shown in Fig. 6 C & D (upper inset). The value of Ipa/Ipc for bioelectrode BSA/anti-FQ/CH-Y_2O_3/ITO was set up to be 0.92, which is almost 1, showing the quasi-reversible electron transfer impending to reversible kinetics [50]. Although for the CH-Y_2O_3 electrode, Ipa/Ipc was set up to be 0.87, indicating the presence of an irreversible transfer progression of electrons. As shown in the upper inset of Fig. 6 C & D, the slopes and intercepts can be determined from Eqs. (S1) to (S4).

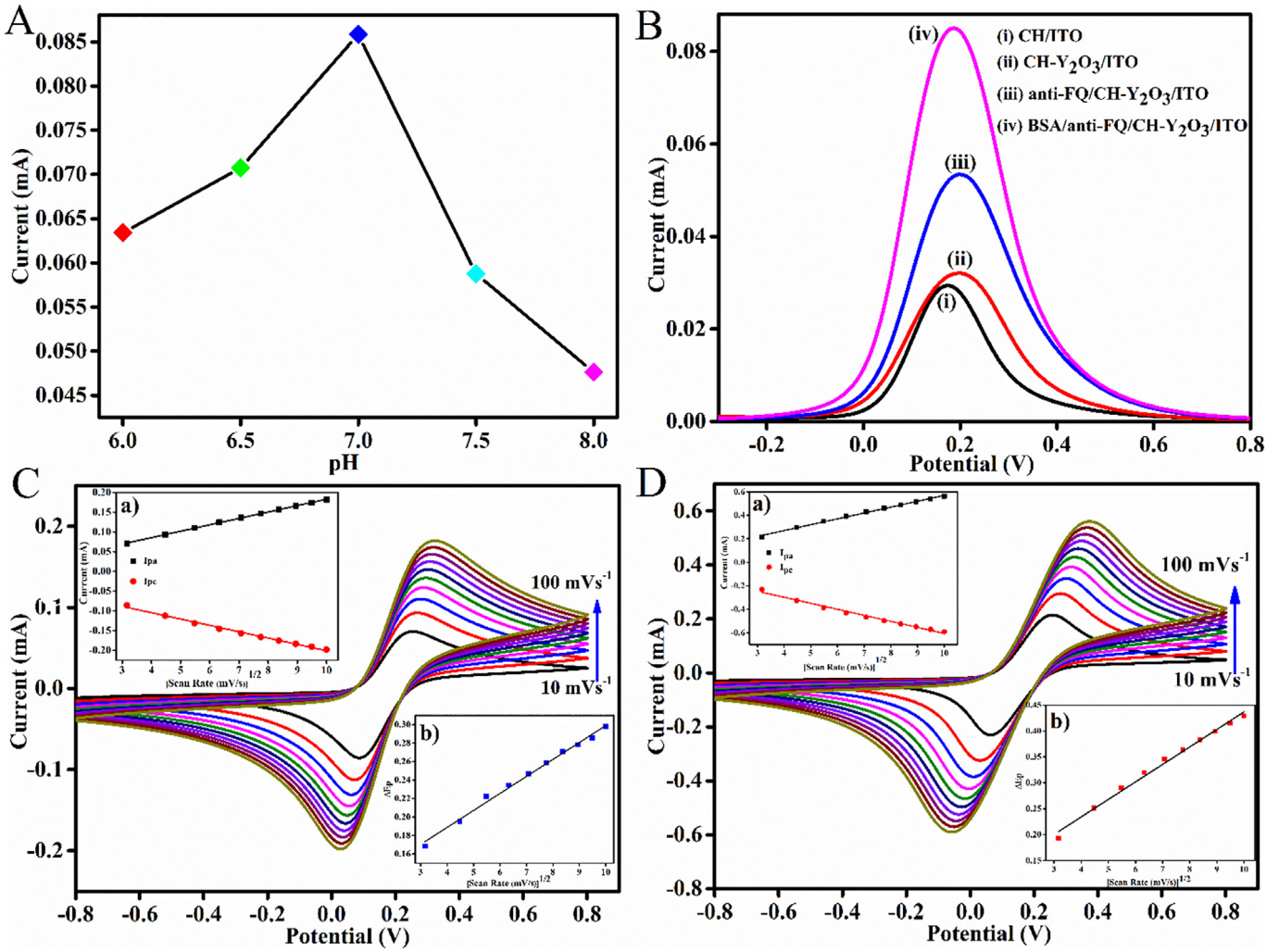

Fig. 6. (A) Effect of pH on BSA/anti-FQ/CH-Y_2O_3/ITO bioelectrode; (B) DPV graph of (i) CH/ITO; (ii) CH-Y_2O_3/ITO; (iii) anti-FQ/CH-Y_2O_3/ITO and (iv) BSA/anti-FQ/CH-Y_2O_3/ITO bioelectrode, (C) *CV* at different scan rates (10–100 mV/s) for CH-Y_2O_3/ITO; and (D) BSA/anti-FQ/CH-Y_2O_3/ITO bioelectrode in PBS with $[Fe(CN)_6]^{3-/4-}$. Corresponding insets showed peak current (I_{pa} and I_{pc}) vs. √scan rate (upper) and peak potentials (E_{pa} and E_{pc}) vs.√scan rate (lower) for respective electrodes.

Moreover, the difference between the cathodic peak potential (E_{pc}) and the anodic peak potential (E_{pa}) [$\Delta E_p = E_{pa} - E_{pc}$] in case of CH-$Y_2O_3$/ITO electrode (0.247) and BSA/anti-FQ/CH-Y_2O_3/ITO bioelectrode (0.346 V), exhibit a linear relationship to the increased scan rate (√υ) as per Eqs. (S5) and (S6) [Fig. 6 C&D (lower inset)], showing a facile electron transfer between the medium and the electrode. The values of kinetic interface factor as diffusion constant (D), surface concentration of redox probe of the electrode (I^*), effective electroactive surface area (A_e), and standard heterogeneous electron transfer rate constant (K_s) for CH-Y_2O_3/ITO electrode and BSA/anti-FQ/CH-Y_2O_3/ITO bioelectrode [57–60] were measured to examine the movement of electrons (Table S1).

3.4. Response studies

To investigate the incubation time for the interaction of NF (100 nM) with BSA/anti-FQ/CH-Y_2O_3/ITO bioelectrodes, the response studies were conducted in the interval of 2 min (Fig. 7A) using DPV. The peak current was observed to decrease from 0 to 8 min, after that, it become constant. These results revealed that the whole interaction of NF with BSA/anti-FQ/CH-Y_2O_3/ITO bioelectrode took approximately 10 min. Thus, 10 min of incubation was given before each measurement for the electrochemical response studies.

The DPV response of the bioelectrode (BSA/anti-FQ/CH-Y_2O_3/ITO) towards NF concentration from 1 pM to10 μM (1 pM, 10 pM, 100 pM, 1 nM, 10 nM, 100 nM, 1 μM and 10 μM) were measured in the potential range from −0.2 V to +0.6 V with incubation time of about 10 min. The decrease in current was found after addition of each NF concentration from 1 pM to 10 μM as the result of the interaction between antigen and antibody on the electrode at the electrolyte interface [Fig. 7B] and became constant after 10 μM. Decrease in the peak current with the addition of NF concentration, was because of the antigen-antibody interaction leads to electrically insulating complex formation, which obstructs the transfer of electrons between bioelectrode and $[Fe(CN)_6]^{3-/4-}$ ions [49]. A 10 μM of NF concentration was found enough for saturating all the antibody molecules present on the bioelectrode. Therefore, the current above this concentration (10 μM) was no longer decreased. Here, 3.87 pM was the lowest concentration of FQ that could be detected, indicating a low detection limit.

Inset of Fig. 7B (b) shows the linear relationship between the change in peak current and the logarithm of NF concentrations [61] gained through DPV. Error bar shows the standard measurement deviations from three independent experiments. Inset of Fig. 7B (c) shows the calibration curve between peak current with NF concentrations from 1 pM to 10 μM. The sensitivity was estimated from the slope of the calibration curve/surface area (0.25 cm^2), as 10.14 μA μM^{-1} cm^2 with R^2 of 0.996 of the linear plots. The bioelectrode lower detection limit has been calculated using the formula 3σ/k, where 'σ' is the standard deviation of the blank electrode and 'k' is the slope of the linear calibration curve given in inset of Fig. 7B. The value obtained is 3.87 pM. These results

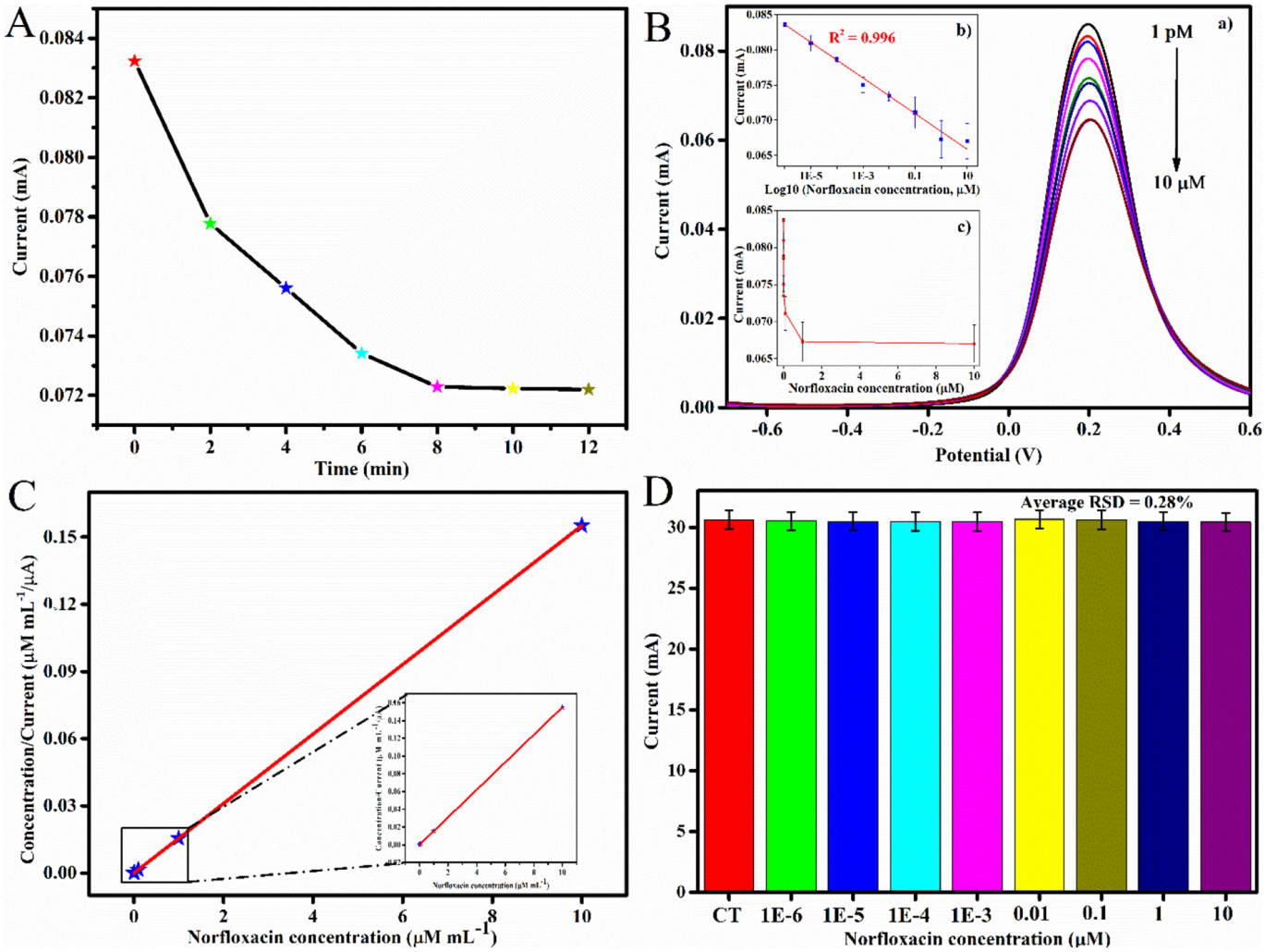

Fig. 7. (A) Incubation time study of BSA/anti-FQ/CH-Y_2O_3/ITO bioelectrode; (B) DPV response studies of BSA/anti-FQ/CH-Y_2O_3/ITO bioelectrode with different NF concentrations in 0.1 M PBS (pH 7.0) containing $[Fe(CN)_6]^{3-/4-}$; (C) Hanes-wolf Graph plot for BSA/anti-FQ/CH-Y_2O_3/ITO bioelectrode; (Inset shows the linearity at lower concentrations (1 pM to 1 μM) and (D) Effect of NF concentration on CH-Y_2O_3/ITO electrode (control study).

reveal the higher sensitivity, low detection limit, and fast response time for the NF detection, and this is comparable to other methods reported in Table 2. These measurements were performed three times to check the repeatability and reproducibility of the sensing study.

The linear plot between peak current and NF concentration provided the equation:

$$\mathrm{Ip} = \left[\left(-2.535\ \mu\mathrm{A}\ \mu\mathrm{M}^{-1}\right) \times \left(\text{conc.of norfloxacin}\ \left(\mu\mathrm{M}^{-1}\right)\right)\right] + 6.84\ \mathrm{mA},\ \mathrm{R}^2 = 0.996 \quad (2)$$

Fig. 7C (Inset shows the linearity at lower concentrations (1 pM to 1 μM) shows the Hanes-wolf plot [(NF conc.) V/s (NF conc/ΔI)] of BSA/anti-FQ/CH-Y_2O_3/ITO bioelectrode. The linearity of the curve is representing the affinity to form immunocomplex in terms of the dissociation constant (K_d). The Hanes-Wolf linear plot equation [62] is given as:

$$\frac{[NOR]}{\Delta I} = \frac{1}{\Delta \mathrm{Imax}}[NF] + \frac{Kd}{\Delta \mathrm{Imax}} \quad (3)$$

where [NF] represents NF conc. in μM mL^{-1}, ΔI (μA) is the DPV peak current, and ΔI_{max} is steady-state current equal to the inverse of the slope (μA). Result of the intercept divided by slope of the linear curve represents the K_d value. The lower bioelectrode K_d value (0.0014 μM mL^{-1}) displays a stronger binding affinity for NF.

To examine the DPV response of the electrode CH-Y_2O_3/ITO with different concentrations of NF, a control experiment had been carried out. No significant electrochemical response with an increased concentration of NF was observed (Fig. 7D). The results suggest that the electrode surface of CH-Y_2O_3/ITO did not respond with the NF antigen.

3.5. Interference, spiked sample, ELISA, shelf-life, reproducibility and repeatability studies

Selectivity is an important parameter for the performance evaluation of the sensor. To assess the biosensor's selectivity possible interfering substances including uric acid [0.03 g 100 mL^{-1}], urea [2 g 100 mL^{-1}], ammonium ions (NH_4^+) [0.05 g 100 mL^{-1}], sodium ions (Na^+) [0.6 g 100 mL^{-1}], chloride ions (Cl^-) [0.6 g 100 mL^{-1}], sulphate ions (SO_4^{2-}) [0.18 g 100 mL^{-1}], potassium ions (K^+) [0.15 g 100 mL^{-1}], phosphate ions (PO_4^{3-}) [0.12 g 100 mL^{-1}], and calcium ions (Ca^{2+}) [0.015 g 100 mL^{-1}] were taken which are generally present in human urine. Firstly, the electrochemical response of BSA/anti-FQ/CH-Y_2O_3/ITO bioelectrode with the NF (100 nM) was carried out by DPV, and after that, uric acid, urea, Na^+, Cl^-, K^+, and Mg^{2+} were added one by one into the same solution and studied the response through DPV. As

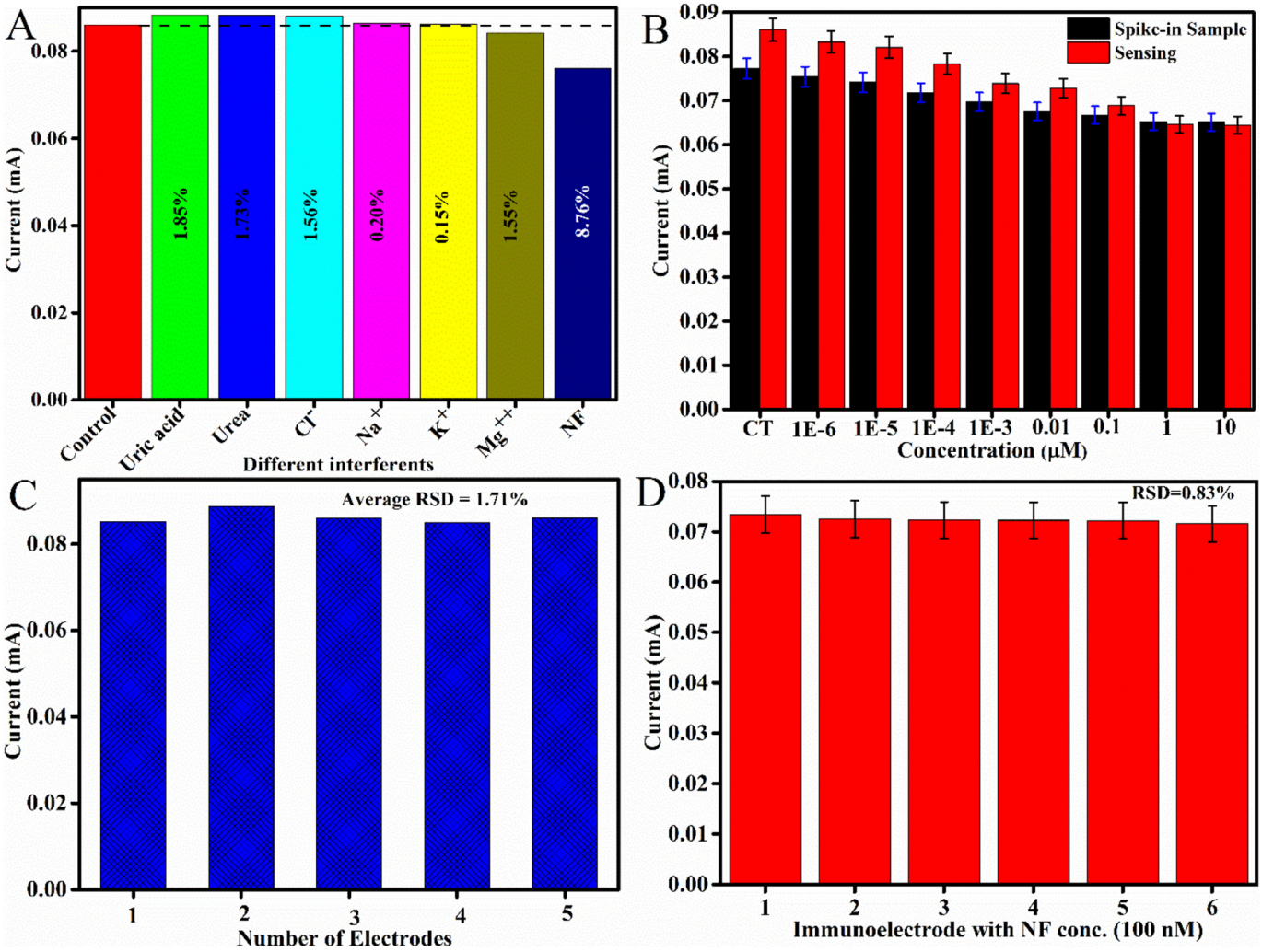

Fig. 8. (A) Effect of different interferent on BSA/anti-FQ/CH-Y_2O_3/ITO bioelectrode; (B) Spiked sample response in comparison with NF; (C) DPV study for reproducibility of BSA/anti-FQ/CH-Y_2O_3/ITO bioelectrode; and (D) Repeatability study of BSA/anti-FQ/CH-Y_2O_3/ITO bioelectrode under similar condition.

depicted in Fig. 8A, BSA/anti-FQ/CH-Y_2O_3/ITO bioelectrode provided low peak current response for NF as compared to all other interferents revealing high specificity.

To further examine the practicability of fabricated BSA/anti-FQ/CH-Y_2O_3/ITO bioelectrode in the real sample, a prepared spiked sample of urine applied to the bioelectrode surface. The percentage of NF recovery and RSD obtained from spiked urine samples (Table 1) was 90.5–101.1% and 0.7–7.04%, respectively, in Fig. 8B. These measured values were quite good, confirming the sensor's accuracy and reliability for the application in real samples.

Table 1
Recovery of NF from human urine samples using BSA/anti-FQ/CH-Y_2O_3/ITO bioelectrode.

NF added to the urine sample	DPV peak current for NOR (μA)	DPV peak current of spike-sample (μA)	Relative standard deviation (%)	Recovery (%)
1 pM	83.34	75.44	7.04	90.5
10 pM	82.09	74.13	7.21	90.3
100 pM	78.34	71.81	6.15	91.7
1 nM	73.91	69.73	4.12	94.3
10 nM	72.78	67.54	5.28	92.8
100 nM	68.85	66.71	2.23	96.9
1 μM	64.64	65.31	0.73	101.1
10 μM	64.48	65.12	0.7	100.1

From Table 2, the fabricated BSA/anti-FQ/CH-Y_2O_3/ITO based bioelectrode has shown better detection limit (3.87 pM) and specificity in comparison to others. The bioelectrode based on BSA/anti-FQ/CH-Y_2O_3/ITO was found to be highly specific with an improved limit of detection for NF as compared to other biomolecule-based electrodes. As far as we are aware, this study represents the first report on electrochemical detection of NF within 10 min with concentration as low as 1 pM and high sensitivity of 10.14 μA μM^{-1} cm^2.

Spiked urine samples were used for the analysis of the BSA/anti-FQ/CH-Y_2O_3/ITO bioelectrode by enzyme-linked immunosorbent assay (ELISA). These samples were processed according to the description given by the ELISA Kit. We measured the concentration of anti-FQ through indirect competitive ELISA Kit (Elabscience, USA) in duplicate. Antigen NF was precoated on the microtiter wells. The colorimetric reaction was observed after completion of all the steps, and the ELISA plate reader showed the absorbance at 450 nm. The concentration versus optical density plot obtained from ELISA Kit and results shown in Fig. S3. Further, the bioelectrode BSA/anti-FQ/CH-Y_2O_3/ITO was found to be more advanced for the detection of norfloxacin owing to its high sensitivity, wide linear range and low limit of detection in comparison with the reported biosensors in literature and enhanced sensitivity and linear range with commercially available ELISA kit as shown in Table 2.

The shelf-life of bioelectrode BSA/anti-FQ/CH-Y_2O_3/ITO has been determined by measuring the change in DPV peak current in PBS of pH 7.0

Table 2
Comparison of BSA/anti-FQ/CH-Y_2O_3/ITO immunosensors with previously reported immunosensors for the detection of NF.

Electrode	Technique	Detection range	LOD	Sensitivity	Incubation time	Storage stability	Ref.
GCE	SWV	15–150 μM	3.5 μM	–	–	–	[20]
MWCNT/GCE	SWV	0.1–100 μM	0.06 μM	–	–	–	[57]
HMDE	LSSV	6–54 μM	0.02 μM	–	–	–	[21]
EPPGS	SWV	5–50 μM	0.28 μM	–	–	–	[19]
CuO/MWCNTs/GC	DPV	1–47.7 μM.	3.21×10^{-7} M	0.028 μA μM^{-1}	–	–	[58]
ELISA	Colorimetric	0.094 pM – 7.609 pM	0.28 pM	0.20 pM/mL cm^{-2}	4–5 h		Elabsci-ence
BSA/anti-FQ/CH-Y_2O_3/ITO	DPV	1 pM-10 μM	3.87 pM	10.14 μA μM^{-1} cm^2	10 min	25 days	Present work

containing 5 mM of $[Fe(CN)_6]^{3-/4-}$ ions at regular interval of 5 days for about 40 days and shown in Fig. S4. Bioelectrode was stored at 4 °C when not in use. It has been found that the bioelectrode retains 96% of its antibody response for 25 days and 84% after 30 days and falls to 82% after 35 days.

Five different bioelectrode of BSA/anti-FQ/CH-Y_2O_3/ITO have been prepared and used individually for reproducibility studies [Fig. 8C]. The reproducibility of the bioelectrode was studied using the DPV technique with NF (100 nM) in a similar set of conditions. In BSA/anti-FQ/CH-Y_2O_3/ITO bioelectrode, the RSD value for reproducibility was found to be 1.71%. The value of bioelectrode reproducibility was in an acceptable range.

The repeatability of the bioelectrode BSA/anti-FQ/CH-Y_2O_3/ITO was examined by measuring the DPV response for a specific concentration (100 nM) of NF [Fig. 8D]. The value of the RSD was observed at 0.83% for consecutive measurements (six times). The result of the BSA/anti-FQ/CH-Y_2O_3/ITO bioelectrode repeatability experiment was satisfactory.

4. Conclusions

BSA/anti-FQ/CH-Y_2O_3/ITO bioelectrode has been successfully prepared for the development of norfloxacin biosensor. nY_2O_3 have been synthesized via a one-step hydrothermal process at low-temperature and were confirmed by using XRD, Raman, TEM, and FTIR. The CH-Y_2O_3 nanocomposite was prepared by the addition of nY_2O_3 (1 mg mL^{-1}) into CH in acetic acid (1%) solution. The CH-Y_2O_3/ITO thin films were fabricated via the drop-casting of 30 μL of CH-Y_2O_3 suspension on ITO surface and used for immobilization of anti-FQ through EDC-NHS coupling. The non-specific sites were blocked by using BSA (blocking agent) for the electrochemical detection of NF. The surface wettability and morphology of fabricated electrodes were examined by the contact angle measurements and FE-SEM study, respectively. CV was performed to observe the oxidation/reduction properties of BSA/anti-FQ/CH-Y_2O_3/ITO bioelectrode. The response of BSA/anti-FQ/CH-Y_2O_3/ITO bioelectrode concerning different concentrations of NF (1 pM-10 μM) was recorded using DPV technique. The results of the studies of bioelectrode have revealed excellent linearity in the range, 1 pM–10 μM (with $R^2 = 0.996$) with NF concentration, high sensitivity 10.14 μA μM^{-1} cm^2, and lower detection limit of 3.87 pM in comparison to biosensors reported previously. The fabricated bioelectrode was found to be very specific to NF. Efforts were made to show the applicability of this sensing platform for real sample analysis in human urine spiked samples and obtained supportive results. The results compared with the ELISA test and earlier described biosensors found better performance in terms of sensitivity and lower detection limit. This bioelectrode based on CH-Y_2O_3 nanocomposite showed a new way to develop highly sensitive, biocompatible and fast responsive biosensors and biochip devices.

Declaration of competing interest

The authors declare that they have no known competing financial interests or personal relationships that could have appeared to influence the work reported in this paper.

Acknowledgment

The authors thank to AIRF, JNU, for their characterization facilities. PRS thanks to the Government of India for financial supports for this work through joint Indo-Russia project (Department of Bitechnology (DBT) DBT/IC-2/Indo-Russia/2017-19/02 and Ministry of Science and Education of Russian Federation, agreement № 14.613.21.0061 by 17.07.2017, unique identification number of the project RFMEFI61317X0061). GBVSL is grateful to Department of Science and Technology (DST), New Delhi, India for DST Women Scientist Project funding (SR/WOS-A/PM-108/2016).

Appendix A. Supplementary data

Supplementary data to this article can be found online at https://doi.org/10.1016/j.ijbiomac.2020.02.089.

References

[1] R. Laxminarayan, R.R. Chaudhury, Antibiotic resistance in India: drivers and opportunities for action, PLoS Med. 13 (2016), e1001974.
[2] P.M. Wehrli, E. Lindberg, T.B. Angerer, A.E. Wold, J. Gottfries, J.S. Fletcher, Maximising the potential for bacterial phenotyping using time-of-flight secondary ion mass spectrometry with multivariate analysis and tandem mass spectrometry, Surf. Interface Anal. 46 (2014) 173–176.
[3] C. Newsroom, Untreatable: Report by CDC Details today's Drug-resistant Health Threats, 2014.
[4] J. Vılchez, O. Ballesteros, J. Taoufiki, G. Sánchez-Palencia, A. Navalon, Determination of the antibacterial norfloxacin in human urine and serum samples by solid-phase spectrofluorimetry, Anal. Chim. Acta 444 (2001) 279–286.
[5] N. Rahman, Y. Ahmad, S.N.H. Azmi, Kinetic spectrophotometric method for the determination of norfloxacin in pharmaceutical formulations, Eur. J. Pharm. Biopharm. 57 (2004) 359–367.
[6] V. More, U. Mote, S. Patil, G. Kolekar, Spectroscopic studies on the interaction between norfloxacin and p-amino benzoic acid: analytical application on determination of norfloxacin, Spectrochim. Acta A Mol. Biomol. Spectrosc. 74 (2009) 771–775.
[7] M.G. Brown, D.L. Balkwill, Antibiotic resistance in bacteria isolated from the deep terrestrial subsurface, Microb. Ecol. 57 (2009) 484.
[8] M.J. Suto, J.M. Domagala, G.E. Roland, G.B. Mailloux, M.A. Cohen, Fluoroquinolones: relationships between structural variations, mammalian cell cytotoxicity and antimicrobial activity, J. Med. Chem. 35 (1992) 4745–4750.
[9] C. Tong, G. Xiang, Sensitive determination of norfloxacin by the fluorescence probe of terbium (III)-sodium dodecylbenzene sulfonate and its luminescence mechanism, J. Fluoresc. 16 (2006) 831–837.
[10] Y. Ni, Y. Wang, S. Kokot, Multicomponent kinetic spectrophotometric determination of pefloxacin and norfloxacin in pharmaceutical preparations and human plasma samples with the aid of chemometrics, Spectrochim. Acta A Mol. Biomol. Spectrosc. 70 (2008) 1049–1059.
[11] H.J. Mascher, C. Kikuta, Determination of norfloxacin in human plasma and urine by high-performance liquid chromatography and fluorescence detection, J. Chromatogr. A 812 (1998) 381–385.
[12] V. Samanidou, C. Demetriou, I. Papadoyannis, Direct determination of four fluoroquinolones, enoxacin, norfloxacin, ofloxacin, and ciprofloxacin, in pharmaceuticals and blood serum by HPLC, Anal. Bioanal. Chem. 375 (2003) 623–629.
[13] R.N. Rao, V. Nagaraju, Separation and determination of synthetic impurities of norfloxacin by reversed-phase high performance liquid chromatography, J. Pharm. Biomed. Anal. 34 (2004) 1049–1056.
[14] J. Lim, B. Park, H. Yun, Sensitive liquid chromatographic–mass spectrometric assay for norfloxacin in poultry tissue, J. Chromatogr. B 772 (2002) 185–189.
[15] A. Espinosa-Mansilla, A.M. De La Pena, D.G. Gómez, F. Salinas, HPLC determination of enoxacin, ciprofloxacin, norfloxacin and ofloxacin with photoinduced fluorimetric (PIF) detection and multiemission scanning: application to urine and serum, J. Chromatogr. B 822 (2005) 185–193.
[16] C. Kowalski, Z. Roliński, T. Sławik, B. Głód, Determination of norfloxacin in chicken tissues by HPLC with fluorescence detection, J. Liq. Chromatogr. Relat. Technol. 28 (2005) 121–135.

[17] G.H. Wan, H. Cui, Y.L. Pan, P. Zheng, L.J. Liu, Determination of quinolones residues in prawn using high-performance liquid chromatography with Ce (IV)–Ru (bpy)$^{32+}$–HNO_3 chemiluminescence detection, J. Chromatogr. B 843 (2006) 1–9.
[18] B. Agrawal, P. Chandra, R.N. Goyal, Y.B. Shim, Detection of norfloxacin and monitoring its effect on caffeine catabolism in urine samples, Biosens. Bioelectron. 47 (2013) 307–312.
[19] R.N. Goyal, A.R.S. Rana, H. Chasta, Electrochemical sensor for the sensitive determination of norfloxacin in human urine and pharmaceuticals, Bioelectrochemistry 83 (2012) 46–51.
[20] M. Ghoneim, A. Radi, A. Beltagi, Determination of Norfloxacin by square-wave adsorptive voltammetry on a glassy carbon electrode, J. Pharm. Biomed. Anal. 25 (2001) 205–210.
[21] Y. Ni, Y. Wang, S. Kokot, Simultaneous determination of three fluoroquinolones by linear sweep stripping voltammetry with the aid of chemometrics, Talanta 69 (2006) 216–225.
[22] N. Prabhakar, H. Thakur, A. Bharti, N. Kaur, Chitosan-iron oxide nanocomposite based electrochemical aptasensor for determination of malathion, Anal. Chim. Acta 939 (2016) 108–116.
[23] M. Hasanzadeh, A. Bahrami, M. Alizadeh, N. Shadjou, Magnetic nanoparticles loaded on mobile crystalline material-41: preparation, characterization and application as a novel material for the construction of an electrochemical nanosensor, RSC Adv. 3 (2013) 24237–24246.
[24] D.K. Sardar, K.L. Nash, J.B. Gruber, A. Sayka, Rare-earth doped nanocrystals for biosensing and imaging, Biophoton. Int. 15 (2008) 45.
[25] L. Mai, N. Boysen, E. Subaşı, T. de los Arcos, D. Rogalla, G. Grundmeier, C. Bock, H.-L. Lu, A. Devi, Water assisted atomic layer deposition of yttrium oxide using tris (N, N′-diisopropyl-2-dimethylamido-guanidinato) yttrium (iii): process development, film characterization and functional properties, RSC Adv. 8 (2018) 4987–4994.
[26] R. Gaboriaud, F. Pailloux, P. Guerin, F. Paumier, Yttrium oxide thin films, Y_2O_3, grown by ion beam sputtering on Si, J. Phys. D. Appl. Phys. 33 (2000) 2884.
[27] S. Kumar, S. Panwar, S. Kumar, S. Augustine, B.D. Malhotra, Biofunctionalized nanostructured Yttria modified non-invasive impedometric biosensor for efficient detection of oral cancer, Nanomaterials 9 (2019) 1190.
[28] G.K. Kouassi, J. Irudayaraj, G. McCarty, Examination of cholesterol oxidase attachment to magnetic nanoparticles, Journal of Nanobiotechnology 3 (2005) 1.
[29] S.F. Wang, Y.M. Tan, A novel amperometric immunosensor based on Fe_3O_4 magnetic nanoparticles/chitosan composite film for determination of ferritin, Anal. Bioanal. Chem. 387 (2007) 703–708.
[30] H.L. Zhang, X.Z. Zou, G.S. Lai, D.Y. Han, F. Wang, Direct electrochemistry of hemoglobin immobilized on carbon-coated Iron nanoparticles for amperometric detection of hydrogen peroxide, Electroanalysis: An International Journal Devoted to Fundamental and Practical Aspects of Electroanalysis 19 (2007) 1869–1874.
[31] A. Kaushik, P.R. Solanki, A.A. Ansari, S. Ahmad, B.D. Malhotra, Chitosan–iron oxide nanobiocomposite based immunosensor for ochratoxin-a, Electrochem. Commun. 10 (2008) 1364–1368.
[32] R. Khan, A. Kaushik, P.R. Solanki, A.A. Ansari, M.K. Pandey, B. Malhotra, Zinc oxide nanoparticles-chitosan composite film for cholesterol biosensor, Anal. Chim. Acta 616 (2008) 207–213.
[33] J. Cruz, M. Kawasaki, W. Gorski, Electrode coatings based on chitosan scaffolds, Anal. Chem. 72 (2000) 680–686.
[34] Y. Miao, S.N. Tan, Amperometric hydrogen peroxide biosensor based on immobilization of peroxidase in chitosan matrix crosslinked with glutaraldehyde, Analyst 125 (2000) 1591–1594.
[35] C. Xu, H. Cai, P. He, Y. Fang, Electrochemical detection of sequence-specific DNA using a DNA probe labeled with aminoferrocene and chitosan modified electrode immobilized with ssDNA, Analyst 126 (2001) 62–65.
[36] I. Kolesnikov, A. Povolotskiy, D. Mamonova, E. Lähderanta, A. Manshina, M. Mikhailov, Photoluminescence properties of Eu^{3+} ions in yttrium oxide nanoparticles: defect vs. normal sites, RSC Adv. 6 (2016) 76533–76541.
[37] Y. Mao, J.Y. Huang, R. Ostroumov, K.L. Wang, J.P. Chang, Synthesis and luminescence properties of erbium-doped Y_2O_3 nanotubes, J. Phys. Chem. C 112 (2008) 2278–2285.
[38] H. Guo, Y.M. Qiao, Preparation, characterization, and strong upconversion of monodisperse Y_2O_3: Er^{3+}, Yb^{3+} microspheres, Opt. Mater. 31 (2009) 583–589.
[39] A. Ubaldini, M.M. Carnasciali, Raman characterisation of powder of cubic RE_2O_3 (RE= Nd, Gd, Dy, Tm, and Lu), Sc_2O_3 and Y_2O_3, J. Alloys Compd. 454 (2008) 374–378.
[40] Y. Repelin, C. Proust, E. Husson, J. Beny, Vibrational spectroscopy of the C-form of yttrium sesquioxide, J. Solid State Chem. 118 (1995) 163–169.
[41] L. Lin, S.A. Starostin, S. Li, S.A. Khan, V. Hessel, Synthesis of yttrium oxide nanoparticles via a facile microplasma-assisted process, Chem. Eng. Sci. 178 (2018) 157–166.
[42] A. Kaushik, R. Khan, P.R. Solanki, P. Pandey, J. Alam, S. Ahmad, B. Malhotra, Iron oxide nanoparticles–chitosan composite based glucose biosensor, Biosens. Bioelectron. 24 (2008) 676–683.
[43] F. Tian, Y. Liu, K. Hu, B. Zhao, The depolymerization mechanism of chitosan by hydrogen peroxide, J. Mater. Sci. 38 (2003) 4709–4712.
[44] M. Aghazadeh, A. Nozad, H. Adelkhani, M. Ghaemi, Synthesis of Y_2O_3 nanospheres via heat-treatment of cathodically grown Y $(OH)_3$ in chloride medium, J. Electrochem. Soc. 157 (2010) D519–D522.
[45] T. Sato, S. Imaeda, K. Sato, Thermal transformation of yttrium hydroxides to yttrium oxides, Thermochim. Acta 133 (1988) 79–85.
[46] M. Aghazadeh, T. Yousefi, M. Ghaemi, Low-temperature electrochemical synthesis and characterization of ultrafine Y $(OH)_3$ and Y_2O_3 nanoparticles, J. Rare Earths 30 (2012) 236–240.
[47] B. Lakshminarasappa, N. Shivaramu, K. Nagabhushana, F. Singh, Synthesis characterization and luminescence studies of 100 MeV Si^{8+} ion irradiated sol gel derived nanocrystalline Y_2O_3, Nucl. Instrum. Methods Phys. Res., Sect. B 329 (2014) 40–47.
[48] L.T.K. Giang, T.K. Anh, L. Marciniak, D. Hreniak, W. Strek, W. Lojkowski, Preparation and characterization of yttrium hydroxide and oxide doped with rare earth ions (Eu^{3+}, Tb^{3+}) nano one-dimensional, Phys. Procedia 76 (2015) 73–79.
[49] S. Tiwari, P.K. Gupta, Y. Bagbi, T. Sarkar, P.R. Solanki, L-cysteine capped lanthanum hydroxide nanostructures for non-invasive detection of oral cancer biomarker, Biosens. Bioelectron. 89 (2017) 1042–1052.
[50] P.K. Gupta, Z.H. Khan, P.R. Solanki, Improved electrochemical performance of metal doped zirconia nanoparticles for detection of Ochratoxin-A, J. Electroanal. Chem. 829 (2018) 69–80.
[51] S. Kumar, J.G. Sharma, S. Maji, B.D. Malhotra, A biocompatible serine functionalized nanostructured zirconia based biosensing platform for non-invasive oral cancer detection, RSC Adv. 6 (2016) 77037–77046.
[52] A. Vasudev, A. Kaushik, S. Bhansali, Electrochemical immunosensor for label free epidermal growth factor receptor (EGFR) detection, Biosens. Bioelectron. 39 (2013) 300–305.
[53] D. Chauhan, P.K. Gupta, P.R. Solanki, Electrochemical immunosensor based on magnetite nanoparticles incorporated electrospun polyacrylonitrile nanofibers for vitamin-D3 detection, Mater. Sci. Eng. C 93 (2018) 145–156.
[54] T.K. Dhiman, G. Lakshmi, A. Roychoudhury, S.K. Jha, P.R. Solanki, Ceria-nanoparticles-based microfluidic nanobiochip electrochemical sensor for the detection of ochratoxin-A, ChemistrySelect 4 (2019) 4867–4873.
[55] A.V. Singh, B.M. Bandgar, M. Kasture, B. Prasad, M. Sastry, Synthesis of gold, silver and their alloy nanoparticles using bovine serum albumin as foaming and stabilizing agent, J. Mater. Chem. 15 (2005) 5115–5121.
[56] A. Singh, R. Patil, M. Kasture, W. Gade, B. Prasad, Synthesis of Ag–Pt alloy nanoparticles in aqueous bovine serum albumin foam and their cytocompatibility against human gingival fibroblasts, Colloids Surf. B: Biointerfaces 69 (2009) 239–245.
[57] J. Singh, A. Roychoudhury, M. Srivastava, P.R. Solanki, D.W. Lee, S.H. Lee, B. Malhotra, A dual enzyme functionalized nanostructured thulium oxide based interface for biomedical application, Nanoscale 6 (2014) 1195–1208.
[58] J. Singh, A. Roychoudhury, M. Srivastava, V. Chaudhary, R. Prasanna, D.W. Lee, S.H. Lee, B. Malhotra, Highly efficient bienzyme functionalized biocompatible nanostructured nickel ferrite–chitosan nanocomposite platform for biomedical application, J. Phys. Chem. C 117 (2013) 8491–8502.
[59] J. Singh, P. Kalita, M.K. Singh, B. Malhotra, Nanostructured nickel oxide-chitosan film for application to cholesterol sensor, Appl. Phys. Lett. 98 (2011), 123702.
[60] J. Singh, P. Khanra, T. Kuila, M. Srivastava, A.K. Das, N.H. Kim, B.J. Jung, S.H. Lee, D.W. Lee, D.-G. Kim, Preparation of sulfonated poly (ether–ether–ketone) functionalized ternary graphene/AuNPs/chitosan nanocomposite for efficient glucose biosensor, Process Biochem. 48 (2013) 1724–1735.
[61] N. Van Chuc, N.H. Binh, C.T. Thanh, N. Van Tu, N. Le Huy, N.T. Dzung, P.N. Minh, V.T. Thu, T. Dai Lam, Electrochemical immunosensor for detection of atrazine based on polyaniline/graphene, Journal of Materials Science & Technology 32 (2016) 539–544.
[62] P.K. Gupta, S. Tiwari, Z.H. Khan, P.R. Solanki, Amino acid functionalized ZrO_2 nanoparticles decorated reduced graphene oxide based immunosensor, J. Mater. Chem. B 5 (2017) 2019–2033.